Sagnac experiment with electrons: Observation of the rotational phase shift of electron waves in vacuum

Franz Hasselbach* and Marc Nicklaus†

Institut für Angewandte Physik, Universität Tübingen, Auf der Morgenstelle 12, D-7400 Tübingen, Germany

(Received 17 November 1992)

A Sagnac experiment with electron waves in vacuum is reported. The phase shift caused by rotation of an electron biprism interferometer placed on a turntable has been measured. It was found to agree with prediction within error margins of about 30%. A compact ruggedized electron interferometer was used. It is based on a high-precision optical bench of 36-cm length. This interferometer is less sensitive by orders of magnitude to mechanical vibrations and electromagnetic stray fields than conventional electron interferometers. A beam of low-energy electrons (150-3000 eV) emitted by a field-emission electron source was used. For the most part, electrostatic electron optical components were employed. The magnified interference fringe pattern was intensified by a dual-stage multichannel-plate intensifier, recorded by a charge-coupled-device video camera, transmitted from the turntable to the laboratory system via a slip ring, and evaluated by an image-processing system. Both the rotation rate and the area enclosed between the two partial waves were varied (up to values of 0.5 s^{-1} and 3.9 mm^2, respectively). Fringe shifts on the order of 5% of a fringe period were attained. Some historical aspects of the Sagnac effect as well as some aspects of its interpretation are mentioned. A brief informal discussion is included of the interpretation of the Sagnac phase shift as a geometric phase ("Berry phase") caused by the global anholonomy of the local phase factor that is produced by the gauge field induced by rotation.

PACS number(s): 03.65.Bz, 03.30.+p, 06.30.Gv, 41.90.+e

I. INTRODUCTION

The effect of rotation on space-time, as it can be measured in two-beam interferometers in which the beams enclose a finite area, is called the Sagnac effect. The first proposal of an interferometrical detection of a rotation, made by Sir Oliver Lodge in 1893 [1] (of course in the context of ether theory), has remained largely unknown. In fact, he proposes to detect the Earth's rotation with a large interferometer and derives an expression for the phase shift that yields the correct result for the Sagnac phase if the transformation is made from ether theory to relativity. In a subsequent paper, he proposes to rotate an interferometer on a turntable [2]. In 1913, Sagnac [3] carried out his famous experiments demonstrating the existence of the effect with a rapidly rotating light-optical interferometer. A few years earlier [4], however, a graduate student in Jena, Franz Harress, very probably had, unknowingly [5,6], observed the Sagnac effect for the first time during his experiments on the Fresnel drag of light. Michelson and Gale [7] demonstrated in 1925 the phase shift caused by the Earth's rotation in a very large light optical interferometer.

After the invention of the laser, the field of light-optical Sagnac interferometry experienced a dramatic increase in precision as well as in width of application. This is demonstrated by devices such as the "ring laser" [8] and the "fiber-optic gyroscope" [9] which are nowadays used in inertial navigation [10].

After a first proposal in 1961 by Heer [11] of a Sagnac experiment with matter waves, Zimmerman and Mercereau performed a Sagnac-type experiment with electron Cooper pairs in 1965 [12]. Both papers do not seem to have become very widely known. After proposals by Page [13] and Anandan [14], the effect of the terrestrial rotation on the neutron phase was demonstrated in 1979 by Werner, Staudenmann, and Colella [15] in a Si perfect-crystal interferometer. The Sagnac-type experiment, using a neutron interferometer of a similar kind rotating in the laboratory, was successfully performed in 1984 by Atwood et al. [16]. Very recently, Riehle et al. [17] have performed a Sagnac experiment with (neutral) ^{40}Ca atom beams.

Clearly then, from a fundamental point of view, an essential gap that remained to be closed in the domain of Sagnac interferometry was the realization of a Sagnac experiment with charged fermions. The neutron interferometrical experiments had shown coupling of the neutron mass to both gravitational [18] and accelerational fields [15, 16, 19] at exactly the same value, thereby proving the validity of the classical principle of equivalence in the quantum limit. Although expected from theory, we felt it to be of fundamental interest and by no means trivial that the presence of charge, with its coupling to the electromagnetic field being so many orders of magnitude stronger, does not influence the electrons' coupling to an accelerational field. It therefore seemed worthwhile to test—within the error margins—this fundamental assumption directly by using charged fermions in vacuum (and thereby avoiding the conceptual difficulties arising from using Cooper pairs, i.e., bosons, interacting with a solid-state device). The development of a very compact and rugged electron interferometer [20] made it possible to conceive of a Sagnac experiment with electrons [21,

22]. The present paper reports on the observation of the phase shift of electron waves in vacuum in a rotating interferometer.

II. THEORY

A. WKB derivation of the Sagnac effect

In order to derive an expression for the phase shift of waves (of any type) in a rotating frame of reference [23], we make the general ansatz

$$\Psi = \Psi_0 \exp\left(\frac{i}{\hbar} S\right) \tag{1}$$

for the wave function, with the action function (phase) S. We assume the waves to be propagating on macroscopical paths so that they can be treated in a semiclassical way using the WKB approximation. A general experimental setup fulfilling this condition would be a source emitting two coherent partial waves which then propagate around a finite enclosed area on macroscopically different paths and interfere with each other at a detector. This condition is certainly fulfilled in the case of the electron interferometer described here with its linear dimensions of tens of centimeters and a separation of the paths of tens of micrometers (whereas the coherence length of the electron waves was on the order of 100 nm).

We want to investigate the effect of the rotationally caused change of the Minkowski metric on the phase difference between the partial waves. From the WKB approximation follows

$$g^{\mu\nu} p_{\mathrm{kin}\mu} p_{\mathrm{kin}\nu} = m^2 c^2, \tag{2}$$

with the metric $g^{\mu\nu}$ and the (kinetic) four-momentum $p_{\mathrm{kin}\mu}$. In the general case of charged particles and the presence of electromagnetic fields, the kinetic four-momentum is

$$p_{\mathrm{kin}\mu} = p_\mu - eA_\mu. \tag{3}$$

The relationship between the canonical momentum p_μ and S is given by

$$p_\mu = \frac{\partial S}{\partial x^\mu} =: S_{,\mu}. \tag{4}$$

We apply the general perturbation ansatz

$$g_{\mu\nu} = \eta_{\mu\nu} + h_{\mu\nu}, \tag{5}$$
$$S = S^{(0)} + S^{(1)}. \tag{6}$$

We assume $h_{\mu\nu}$ to be a small perturbation of a general kind of the unperturbed Minkowski metric of flat space. This does not yet necessarily have to be a perturbation caused by rotation. From Eqs. (5), (3), and (4) follows

$$p_{\mathrm{kin}\mu} = S^{(0)}_{,\mu} - eA_\mu + S^{(1)}_{,\mu}, \tag{7}$$

and with

$$S^{(0)}_{,\mu} - eA_\mu = p^{(0)}_{\mathrm{kin}\mu} \tag{8}$$

we further obtain

$$p_{\mathrm{kin}\mu} = p^{(0)}_{\mathrm{kin}\mu} + S^{(1)}_{,\mu}. \tag{9}$$

Applying this and (5) to (2), we obtain

$$(\eta^{\mu\nu} + h^{\mu\nu})(p^{(0)}_{\mathrm{kin}\mu} + S^{(1)}_{,\mu})(p^{(0)}_{\mathrm{kin}\nu} + S^{(1)}_{,\nu}) = m^2 c^2, \tag{10}$$

using the contravariant components of the metric. In keeping with the assumption of a small perturbation, we retain only the terms of first order in $g^{\mu\nu}$ and S combined and obtain

$$2\eta^{\mu\nu} S^{(1)}_{,\mu} p^{(0)}_{\mathrm{kin}\nu} + h^{\mu\nu} p^{(0)}_{\mathrm{kin}\mu} p^{(0)}_{\mathrm{kin}\nu} = 0, \tag{11}$$

or, equivalently, using the covariant components $h_{\mu\nu}$,

$$p^{(0)\mu}_{\mathrm{kin}} S^{(1)}_{,\mu} = -\frac{1}{2} h_{\mu\nu} p^{(0)\mu}_{\mathrm{kin}} p^{(0)\nu}_{\mathrm{kin}}. \tag{12}$$

Parametrizing the unperturbed wave path,

$$p^{(0)\mu}_{\mathrm{kin}} =: \frac{dx^\mu}{d\lambda}, \tag{13}$$

(12) transforms to

$$\frac{dx^\mu}{d\lambda} S^{(1)}_{,\mu} = \frac{d}{d\lambda} S^{(1)} = -\frac{1}{2} h_{\mu\nu} \frac{dx^\mu}{d\lambda} \frac{dx^\nu}{d\lambda}. \tag{14}$$

The phase difference between the two partial waves is given by the integral of the action along the closed path surrounding the encircled area. This yields the phase shift

$$\Delta\varphi = \frac{1}{\hbar} \oint \frac{dS^{(1)}}{d\lambda} d\lambda = -\frac{1}{2\hbar} \oint h_{\mu\nu} \frac{dx^\mu}{d\lambda} \frac{dx^\nu}{d\lambda} d\lambda, \tag{15}$$

caused by the perturbation.

We now, more specifically, assume the perturbation to be a rotation of the frame of reference. From the line element of a rotating coordinate system

$$ds^2 = c^2 dt^2 - d\mathbf{r}\cdot d\mathbf{r} - 2(\mathbf{\Omega}\times\mathbf{r})\cdot d\mathbf{r}dt, \tag{16}$$

we immediately derive

$$-2(\mathbf{\Omega}\times\mathbf{r})\cdot d\mathbf{r}dt = h_{\mu\nu} dx^\mu dx^\nu, \tag{17}$$

and further

$$h_{\mu\nu} \frac{dx^\mu}{d\lambda} \frac{dx^\nu}{d\lambda} = -2(\mathbf{\Omega}\times\mathbf{r})\cdot\frac{d\mathbf{r}}{d\lambda}\frac{dt}{d\lambda}. \tag{18}$$

Observing

$$E/c = p^{(0)0}_{\mathrm{kin}} = \frac{c\,dt}{d\lambda}, \tag{19}$$

we obtain the general expression

$$\Delta\varphi = \frac{1}{\hbar c^2} \oint (\mathbf{\Omega}\times\mathbf{r})E\cdot d\mathbf{r} \tag{20}$$

for the rotationally induced phase shift between two partial waves whose corresponding particles have the total energy E. In the general case, E may be variable along the path. In all practical Sagnac interferometers, E is constant along the path to a very good approximation. This is certainly the case in the electron interferometer

used in this experiment, where all changes in kinetic energy along the beam path are small [24] compared to the rest energy of the electrons (511 keV). Since Ω, too, is constant along the path in all practical realizations of Sagnac interferometers, we can pull E and Ω out of the integral. We thus obtain the Sagnac phase shift

$$\Delta\varphi = \frac{E}{\hbar c^2}\Omega\cdot \oint (\mathbf{r}\times d\mathbf{r})$$
$$= \frac{2E}{\hbar c^2}\Omega\cdot\mathbf{A}. \qquad (21)$$

B. Remarks

A number of comprehensive articles [14, 25–28] have described various aspects of the Sagnac effect and have also undertaken to elucidate the conceptual difficulties that seem to be encountered in its interpretation. Various authors have derived the Sagnac phase shift in a number of ways: by optical analogy [13], general relativity considerations [10, 29, 30], special relativity analyses [28, 31–35], the WKB approximation [15], the Doppler effect of moving media in an inertial frame [36], a classical kinematical derivation [22, 37–39], dynamical analysis in a noninertial frame [40, 41], by analogy with the Aharonov-Bohm effect [42], by extension of the hypothesis of locality [43], by adiabatic invariance [44], using ether concepts [45], and in other ways. This great variety (if not disparity) in the derivation of the Sagnac phase shift constitutes one of the several controversies (recounted, e.g., in [31, 46, 47]) that have been surrounding the Sagnac effect since the earliest days of studying interferences in rotating frames of reference.

The classical kinematical derivation, as it has been used by many authors (see above), has the advantage of yielding the correct first-order result in a very simple and intuitive way. Its starting point is a consideration that applies to any type of waves, and it seems entirely classical. Consider a circular path with radius R. Two counterpropagating coherent wave packets are emitted from the same starting point, and circulate around the enclosed area A with the velocity u. After a full circulation by each partial wave, their interference pattern is observed at the starting point. In the case of rotation of the whole system with angular velocity Ω, the co-rotating point of observation will have moved the short distance $\Delta s = R\Omega t$ towards one of the waves, and the same distance Δs away from the other one. The time for one circulation is $t\approx \frac{2\pi R}{u}$, with the experimentally fulfilled assumption $R\Omega \ll u$. A total path-length difference $\Delta l = 2\Delta s = 4\pi \frac{R^2\Omega}{u}$ results, which translates into a phase $\Delta\varphi = \frac{8\pi}{\lambda u}A\Omega$. Substituting $\lambda = h/p$ and $E = mc^2$ in the case of matter waves, one obtains $\Delta\varphi_{\mathrm{mat}} = \frac{8\pi}{h c^2}EA\Omega$. These final substitutions, however, $E = mc^2$ and $\lambda = h/p$, are the inherently nonclassical steps [48] that introduce the decisive element of relativity. It is this covertly relativistic feature of nonrelativistic quantum mechanics [34] that defines the scope of this derivation, and Anandan has shown [26] that precisely for this reason there is no Sagnac effect at all if electrons

are treated as classical particles in a nonrelativistic way. This necessity for limiting the application of the term "Sagnac effect" to the intrinsically relativistic effect, and for differentiating it from competing effects such as the Fizeau-Fresnel drag, has been the source of another ongoing controversial discussion [5, 6, 49]. This point becomes immediately evident [34, 39] if one would—erroneously—apply the kinematical derivation to sound waves. It has been argued, therefore, that the Sagnac effect is a purely "topological" effect [50], resulting from the effect of rotation on the geometry of space-time. This becomes even more evident if one considers the close analogy [30, 34, 42, 51] of the Sagnac effect with the Aharonov-Bohm effect [52, 53]; and both, in turn, are manifestations of the "geometric" and/or "topological" phase [54] picked up by a quantum-mechanical system transported adiabatically [55] around a closed circuit in parameter space, the so-called Berry phase [56]. This phase, which is picked up in addition to the usual dynamical phase, depends only on the geometric history of the system, and reflects the global nonintegrability (or anholonomy) of the local phase factor produced by a gauge field ("phase-shift field" [57]). In the Sagnac experiment, the two partial beams enclosing the finite area A represent the cyclic evolution of the system, and the rotation provides the curvature of the (parameter) space around which the parallel transport of the electron states takes place. Here, in fact, the parameter space is identical to the three-dimensional space (or to space-time; see below). The Sagnac effect is not as "fully topological" [58] as, e.g., the Aharonov-Bohm effect [since the electrons are not traveling in (Coriolis-) force field-free regions (see, however, e.g., [59, 60] for proposals of experiments that would fulfill this requirement)]. It can nevertheless be attributed topological characteristics in the following sense.

(1) The Sagnac phase is valid for any path encircling the enclosed area A, as long as this area (or more exactly, the projection of $\mathbf{A}$ onto Ω) remains constant.

(2) The location of A relative to the axis of rotation is irrelevant.

(3) For massive particles, it is independent of their kinetic energy in the low-energy ("nonrelativistic") limit [since in Eq. (21) E denotes the total, not only the kinetic energy].

Chiao [54] has called this type of anholonomy, which underlies the Sagnac effect, "age anholonomy," and has also pointed out its close analogy with the twin paradox of relativity (see also [34, 61]).

The question whether the Sagnac effect can only be treated adequately in the framework of general relativity (as opposed to a special relativistic treatment being sufficient), has perhaps generated the most extensive controversial discussion in this field. Many authors have argued for either point of view (see the references cited above), and this has even led some to talk of an "intermediate" character of the Sagnac effect [62]. To a certain degree, some of the controversy seems to be a problem of definition rather than of physics. It seems to have become increasingly accepted, however, that the Sagnac effect can be seen as special relativistic insofar as a rotation alone

(i.e., without masses being present), although causing the system to become noninertial, does not alter a previously flat Minkowski space-time, i.e., the four-dimensional geometry remains pseudo-Euclidean [31,35]. The geometry of the *three*-dimensional space, however, can be thought of becoming non-Euclidean in this case, i.e., acquiring a curvature. The perturbation of the metric caused by rotation can be shown to be replaceable by a series of Lorentz transformations and translations [26], and both are formally equivalent when expressed in cylinder coordinates [38]. Therefore the Sagnac effect, as measured in an interferometrical setup as illustrated in Fig. 2, can be interpreted as the result of the special relativistic length contraction of the wave paths. The equivalent impossibility of globally synchronizing clocks in a rotating frame of reference was already noted by Einstein [63]. It was experimentally proved with the famous "flying clocks" [64], and with electromagnetic signals transmitted around the earth [33, 65], which both demonstrated the existence of the Sagnac effect on a global scale.

III. EXPERIMENT

A. Experimental conditions and difficulties

The task at hand when performing a Sagnac experiment with free-electron waves (i.e., with electron beams in vacuum, as opposed to, e.g., electron Cooper pairs traveling in a solid-state device) is to rotate an entire electron optical setup still capable of delivering a detectable electron interference pattern while under rotation. The wave path-length differences to be expected in our experiment were on the order of 10^{-12} m, and the ensuing phase shifts on the order of 5% of a fringe period. This meant that the phase had to be measured with a sensitivity of 1% of a fringe period or better in order to keep the error introduced by the registration process within acceptable limits, and that the interference pattern had to be stable for the duration of the experiment to a degree comparable to the expected phase shift.

Electron interferometers are substantially more sensitive in two crucial aspects when compared to light optical interferometers and, to a lesser extent, neutron- and atom-beam interferometers. The short electron wavelength (of only fractions of a nanometer) makes them extremely sensitive to mechanical vibrations. The electrons' charge (in contrast to photons, neutrons, and neutral atoms) renders electron interferometers very sensitive to ambient electromagnetic fields, which range from the Earth's magnetic field through ac magnetic stray fields to radio-frequency electromagnetic fields. The low-electron energies used in our interferometer (the reasons for that are given later) make the influence of such fields even more significant. The unavoidable instabilities and noise of the electronic circuitry supplying the voltages and currents to the electron optical components represent a further limitation in electron interferometry. Specific to a Sagnac electron interferometer, the Aharonov-Bohm effect yields an increasing sensitivity to ac magnetic stray fields proportional to the enclosed area, which, on the other hand, should be as large as possible for observation of the Sagnac effect.

For these reasons, the maximum attainable enclosed area A between the coherent partial beams is much smaller in electron interferometers (usually on the order of a few mm^2) than in light optical or neutron interferometers. This makes relatively high rotation rates on the order of 1 s^{-1} necessary in order to obtain detectable Sagnac phase shifts. Any electron optical setup can only operate in high vacuum, and the use of a field-emission electron source in our interferometer, which will be detailed later, even necessitated an ultrahigh-vacuum (UHV) environment. The difficulties encountered in UHV with any mechanical devices, such as motors, as well as the constraints imposed by the interference image registration process, made it impossible to rotate solely the electron optical setup within the vacuum chamber. Consequently, the entire vacuum system had to be rotated. The relatively high rotation rates mentioned earlier lead to centrifugal effects, such as minute bending of the vacuum chamber, that can cause shifts of the whole interference pattern in the registration plane simulating phase shifts of the same magnitude as the expected Sagnac phase shift. Finally, in contrast to electron microscopy with its usual exposure times of a few seconds, a long term stability of at least 10 min was needed because of the relatively long time periods needed for rotationally accelerating and decelerating the whole heavy apparatus, and because of the registration procedure that had to be adopted.

B. Experimental setup

A novel type of electron biprism interferometer was used. It has been described in detail previously [20]. Its design focuses on rigidity and compactness in order to reduce the sensitivity of the interferometer to the aforementioned influences. Its construction principle is basically that of a high-precision miniaturized optical bench. All electron optical components are of circular cross section and have a diameter of 28 mm. They are very tightly fixed to two high-precision ceramic rods (8-mm diameter) by a special brace construction. The entire optical bench has a length of only about 36 cm. Due to this compact and rigid design, vibrational eigenfrequencies of the interferometer were achieved that were high enough (>100 Hz) to virtually eliminate its sensitivity to all ambient mechanical vibrations such as those transmitted along the building's floor (typically between 1 and 10 Hz).

The optical bench principle using the geometry described above, when combined with narrow fabrication tolerances, affords an excellent coarse alignment of the electron optical components onto a common optical axis. Tolerances in the diameter of those components on the order of 10 μm were achieved. Therefore, large-scale mechanical alignment is not necessary (and would be difficult to reconcile with the requirement of mechanical rigidity). Consequently, no mechanical alignment facil-

ities are provided, which eliminates the need for any mechanical feedthroughs. Due to this and to the instrument's compactness, a very efficient magnetic shielding could be achieved. A high permeability alloy cylinder without any lateral bores surrounded the entire optical bench inside the vacuum chamber. A residual orientation-dependent beam deflection caused by the Earth's magnetic field was eliminated by several additional magnetic shields placed inside and outside the vacuum chamber. The last of those was a box [71 cm (width)×116 cm (depth)×50 cm (height)] made out of high permeability material encasing the entire vacuum chamber. The total magnetic shielding factor achieved was on the order of 250 000. A schematic diagram of the entire apparatus positioned on the turntable is shown in Fig. 1.

The electron optical setup that was used is shown in Fig. 2(a), the beam path in Fig. 2(b). Low-energy electrons (150–3000 eV) emitted from a diode field-emission gun were used. The use of a field-emission source has a decisive advantage over a thermionic electron source insofar as it offers (1) a much smaller virtual source size, which helps avoid a loss of contrast in the interferogram due to insufficient spatial coherence, and which allows us to do without a demagnification stage; (2) a much higher beam brightness, which guarantees sufficient intensity in the interference pattern even at high magnifications; and (3) a smaller energy spread, which increases temporal coherence of the partial wave packets. Furthermore, field-

FIG. 2. (a) Electron optical setup of the interferometer. (b) Electron-beam path viewed along the biprism filaments, i.e., the filaments are to be thought perpendicular to the plane of the drawing. The dimensions of the interferometer are given in mm along the bottom.

emission sources can be built in a constructionally more simple form (see below) than thermionic sources. On the other hand, the emission process of most field-emitter types available today suffers from unavoidable emission current fluctuations, which are typically on the order of 10%, and often substantially higher. Those fluctuations constituted the major contribution to the error margins of the experiment.

The emitter was a $\langle 100 \rangle$-oriented tungsten single crystal, which was electrolytically etched [66, 67] into a very fine tip (curvature at the apex typically < 50 nm). Its shape could be influenced and, if necessary, restored to optimum emission conditions by simultaneously applying an inverse electric field and heat to the emitter in a so-called "remolding" process [68, 69]. The total field-emission currents varied widely. An optimal compromise between image brightness and stability of the emission could, however, often be achieved with emission currents in the range of 20–100 nA. No further acceleration of the electrons was provided besides that produced by the field-emission extraction voltage. This ensures maximum compactness of the electron gun (total length 34 mm), and allowed using very compact components for the subsequent electron optics. Furthermore, higher electron energies would lead to undesirably small wavelengths. Finally, the use of only one anode ensures a minimum virtual source in contrast to the conventionally used triode systems where the additional anode unavoidably adds aberrations. On the other hand, the use of a diode system does not allow one to chose the electron energy independent from the emission current. The problem that this poses with the adjustment of the electron optics was solved by electronically coupling [39] the voltage and current supplies with the field-emission extraction voltage. The UHV necessary for the operation of the field-emission source was provided by a 30 l/s ion-getter pump, which maintained a vacuum of $\sim 5 \times 10^{-10}$ hPa.

Most of the electron optical components of the interferometer use electrostatic rather than magnetic fields. This
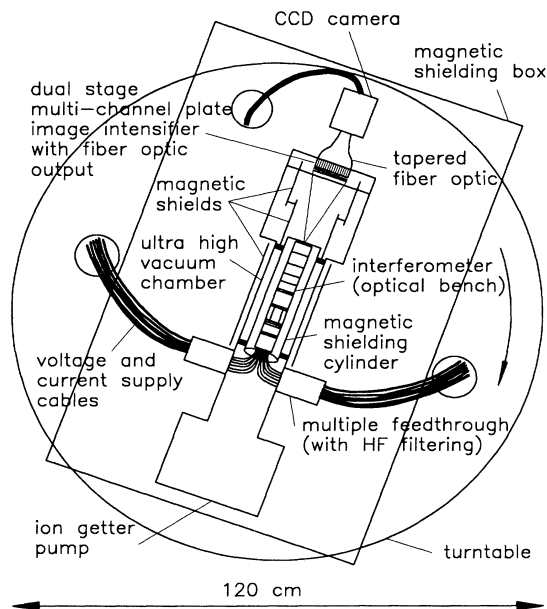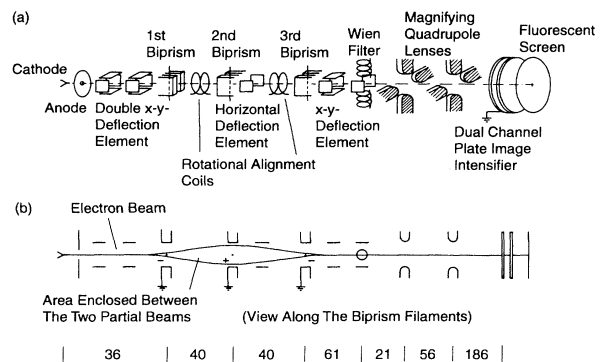

FIG. 1. Schematic diagram of the entire apparatus positioned on the turntable. The view is along the rotation axis of the turntable. The cables supplying voltages and currents to the interferometer as well as the camera cable are connected through holes in the upper plate of the turntable to the electronic circuitry (see text) corotating on a lower plate of equal diameter. Height above ground of the lower plate: 34 cm; distance between lower and upper plate: 60 cm.

was chosen mostly because electrostatic electron optics can be built in a simpler and more compact way. Electrostatic deflection systems are used for fine alignment of the electron beam. The coherent wave fronts are made to diverge by a negatively charged filament (Möllenstedt electron biprism [70, 71]). A second filament, which is positively charged, causes them to converge again (and thus to enclose a finite area), and to form interference fringes in the region of overlap. The electron wave fronts leaving the first biprism can be rotated by alignment coils [72] which produce a weak longitudinal homogeneous magnetic field. This is necessary in order to align the wave fronts with the direction of the second biprism filament, since it is usually impossible to mount the two filaments exactly parallel to each other.

The angle of deflection in a Möllenstedt electron biprism, which is constant for all incoming electron trajectories [71], is given by

$$\beta = \frac{\pi}{2} \frac{1}{\ln(R/r)} \frac{U_f}{U_a}, \tag{22}$$

where R is the distance between the filament and the earth electrode, r is the filament radius, U_a is the acceleration voltage, and U_f is the voltage applied to the filament. R was 2 mm, and r was on the order of 1 μm (but see below). The total size of the enclosed area, $A = A_0 + A_1 + A_2$, as shown in Fig. 3, can easily be calculated as

$$A = ar + l^2 \tan(\alpha_0 + \beta_1) \left(1 + \frac{\tan(\alpha_0 + \beta_1)}{\tan(\beta_2 - \beta_1 - \alpha_0)}\right), \tag{23}$$

where the symbols are the same as the ones used in Fig. 3. Using Eq. (22), and making a few approximations [39], A can be expressed in experimental parameters as

$$A = \frac{\pi}{2} \frac{1}{\ln(R/r)} \frac{l^2}{U_a} \frac{U_{f1}U_{f2}}{U_{f1} + U_{f2}}, \tag{24}$$

where U_{f1} and U_{f2} are the voltages at the biprism filaments of the first and the second biprism, respectively.
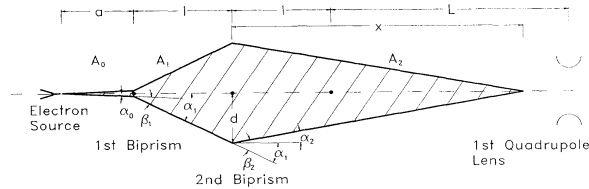

FIG. 3. Geometry of the enclosed area A. The distance from the cathode tip to the first biprism filament was $a \approx$ 36 mm, the distance between the first and the second biprism filament was $l = 40$ mm, and the distance from the second biprism filament to the first magnifying quadrupole lens was $L = 82$ mm. The beam separations achieved were on the order of $2d = 20$–60 μm. The distance x between the second biprism filament and the beginning of the region of overlap is determined by the deflection angles β_1 and β_2, and is typically somewhat smaller than $l + L$.

The impossibility of exactly determining the filament radii as well as some other effects (such as secondary electron emission from and to the filaments) causing uncertainties as to the effective potential of the filaments [39] resulted in an error margin for A of 10–20 %.

A third biprism filament is available for, e.g., reducing the angle of superposition of the two partial waves if a negative voltage is applied. It was, however, not used in the experiments that yielded the results reported below. With the de Broglie wavelengths of the electron beams used on the order of $\lambda = 0.3$ Å, and beam separations achieved of 20–60 μm, the fringe spacings in the primary interference field were on the order of 50–150 nm.

In massive particle interferometry, coherence lengths are usually very short (typically in the range of 10–1000 nm) due to the small de Broglie wavelengths and the unavoidable energy spread of particle beams (0.3–0.4 eV in the case of the field emitter used here). The intrinsically dispersive propagation of such de Broglie waves even in vacuum, which causes an increase in the spatial extent of the wave packet as it propagates down the wave path, does, however, not increase the coherence length available for producing an observable interference pattern [73]. For this reason, a Wien filter was placed in the beam path in order to allow optimization of the fringe contrast by shifting the two wave packets relative to each other longitudinally [74]. Its crossed electrostatic and magnetic fields, both perpendicular to each other and the beam path, provoke a shift of the wave packets relative to each other along the beam path without causing any deflection nor phase shift if the fields are suitably matched so that the electrostatic (Coulomb) and the magnetic (Lorentz) forces exactly cancel. The necessity for such an application of a Wien filter as well as theoretical background and constructional and experimental details are recounted in the companion paper [75].

The need of accommodating for a large range of electron energies on the one hand (see above) combined with the high stability requirements in electron interferometry on the other hand resulted in very high demands on the stability of the voltage and current supplies. The deflection elements and the Wien filter are the most critical components in this respect. In order to limit fringe shifts caused by those voltage and current fluctuations to 1% of a fringe, a relative stability of the supply modules of on the order of 5×10^{-8} relative to the maximum output would have been necessary. Stability values of up to 5×10^{-7} for short-term (> 1 Hz) fluctuations could be achieved using specifically designed circuitry and modified commercial modules. The fringe shifts caused by those fluctuations were averaged out by the registration procedure described below. The long-term drifts could be held sufficiently low to allow the measurements reported in Sec. IV, but constituted one of the contributions to the error margins of the experiment.

The primary interference fringes were magnified by two electrostatic quadrupole lenses. The magnified interference image was intensified by a dual-stage channelplate image intensifier which was equipped with a fiberoptic UHV image throughput coated with a P20 phosphor. From the intensifier's fiber-optic output, the im-

age was transferred via a tapered fiber optic to a video camera that was equipped with a high-sensitivity charge-coupled-device (CCD) sensor.

The UHV chamber, including the ion-getter pump, was mounted on a rotating table (see Fig. 1), as were all interferometer controls, the power supplies providing currents and voltages to the electron optical components, and the CCD camera control. This was done in order to eliminate the need for the line voltage transmission to the turntable during rotation, which would have required both increased safety measures and increased measures to block the ac line frequency from interfering with the experiment. To allow this, the entire interferometer could be switched to power supply from batteries only, and those batteries (12-V lead accumulators) were also positioned on the rotating table. Details of this setup are described in [39]. The diameter of the turntable was 120 cm. The total rotating mass was about 300 kg.

The rotating table was driven by an electronically controlled dc motor via a V-belt. Centrifugal forces acting on the vacuum chamber caused minute bending of the interferometer, resulting in lateral shifts of the interferogram in the registration plane. In order to avoid any such influence of centrifugal forces on the Sagnac experiments, we measured the phase differences between successive alternating clockwise and counterclockwise rotations at exactly the same absolute rotation rate. The time for successively accelerating the turntable, registering the interferogram, decelerating the turntable, and inverting the sense of rotation was 30–60 s (depending on the rotation rate).

The CCD sensor used had 576(V)× 384(H) picture elements (pixels). In order to increase the signal-to-noise ratio (SNR) in the interferograms and to average over the mentioned residual, orientation-dependent shifts of the interference field caused by the Earth's magnetic field, the image was accumulated on the CCD sensor during multiple integers of the rotation period.

The video signal was transferred to the laboratory system via a slip ring. It was transmitted to an image-processing system that had a video frame memory with an image page size of 512×512×8 bits. The phase information was extracted from the interference pattern in the following way.

The CCD camera was mechanically aligned with the interference image so that the pixel columns of the CCD sensor were parallel to the fringes. This allowed the information in all pixels of one column to be summed up by the image-processing system to yield a spatial integration of the interferogram. Thereby the SNR is increased by
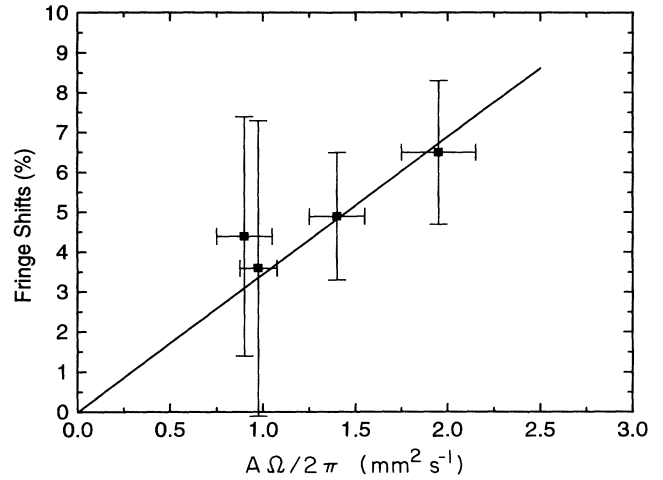

FIG. 4. Experimentally observed fringe shifts for variation of both the enclosed area A and the rotation rate $\Omega/2\pi$, as listed in Table I. The fringe shifts are given in units of percent of a fringe period. The horizontal error bars result from the uncertainty in determining the enclosed area A (see text). Also shown is the theoretically predicted Sagnac phase shift (solid line).

a factor equal to the square root of the number of image memory rows per interferogram [multiple interferograms (up to 16) were stored in multiple horizontal sections of one image frame, thus reducing the number of image memory rows per interferogram to a fraction of 512]. The numerical result of both the temporal accumulation on the CCD sensor and the spatial integration in the image-processing system is a one-dimensional low-noise densitometer trace across the interference field. This trace was Fourier analyzed, and the phase information was calculated via the arctan of the Fourier components of the intensity distribution $I(x)$,

$$C = \int_{-\infty}^{+\infty} I(x) \, \cos(2\pi f_0 x) \, dx \tag{25}$$

and

$$S = \int_{-\infty}^{+\infty} I(x) \, \sin(2\pi f_0 x) \, dx, \tag{26}$$

yielding

$$\varphi = \arctan(S/C), \tag{27}$$

TABLE I. Experimental parameters and results for each measurement.

No.	U_a (V)	U_{f1} (V)	U_{f2} (V)	A (mm^2)	$\Omega/2\pi$ (s^{-1})	Rotation-sense reversals	$\Delta\phi_{\text{theor}}$ (%)	$\Delta\phi_{\text{expt}}$ (%)
1	-1174	-2.17	+3.35	1.8 ± 0.3	0.5	5	3.11 ± 0.54	4.4 ± 3.0
2	-1721	-4.60	+6.71	2.8 ± 0.3	0.5	7	4.89 ± 0.60	4.9 ± 1.6
3	-1721	-6.01	+8.47	3.9 ± 0.4	0.5	7	6.81 ± 0.78	6.5 ± 1.8
4	-1721	-6.01	+8.47	3.9 ± 0.4	0.25	8	3.40 ± 0.39	3.6 ± 3.7

where f_0 is the spatial frequency of the interference fringes. By using a Hanning window [76] in the sampling of $I(x)$, a phase error of less than 1% of a fringe period could be achieved for the registration process, with a typical total number of electrons in one interferogram of ca. 40 000.

IV. RESULTS

The main difficulties introducing the errors in the experiments were the instabilities of the field-emission current and, to a lesser degree, of the currents and voltages fed to the electron optical components. In order to improve on the statistics of the measurements, phase differences were averaged over a series of successive rotation sense reversals. The maximum number of those reversals per series was limited by the long-term instabilities of the field-emission process. A total of four such series of rotation-sense reversals could be obtained in which the standard deviation of the averaged phase difference did

not substantially exceed the mean value. Details of those measurements have been reported elsewhere [77]. Both the enclosed area A and the rotation rate Ω were varied, and the number of rotation-sense reversals ranged from 5 to 8. Table I gives the experimental parameters used, and the expected and the measured phase shifts. The substantially larger error in measurement No. 4 may have been produced by minute mechanical destabilization in the interferometer caused by the preceding rotation experiments. Figure 4 shows that the phase shifts measured are in good agreement with the theoretically expected values for the Sagnac phase shift.

ACKNOWLEDGMENTS

* To whom correspondence should be addressed.
† Present address: National Cancer Institute, National Institutes of Health, Bethesda, MD 20892.

[1] O. J. Lodge, Philos. Trans. R. Soc. London **184**, 727 (1893).

[2] O. J. Lodge, Philos. Trans. R. Soc. London **189**, 149 (1897).

[3] G. Sagnac, C. R. Acad. Sci. **157**, 708 (1913); **157**, 1410 (1913); J. Phys. (Paris) **4**, 177 (1914).

[4] F. Harress, Ph.D. thesis, University of Jena, Germany (1912). This publication has been reported by several authors as being unavailable or even lost. It is available in the Library of the University of Tübingen.

[5] P. Harzer, Astron. Nachr. **198**, 377 (1914).

[6] A. Einstein, Astron. Nachr. **199**, 7 (1914).

[7] A. A. Michelson and H. G. Gale, assisted by F. Pearson, Astrophys. J. **61**, 137 (1925).

[8] W. M. Macek and D. T. M. Davis, Jr., Appl. Phys. Lett. **2**, 67 (1963).

[9] V. Vali and R. W. Shorthill, Appl. Opt. **15**, 1099 (1976).

[10] W. W. Chow *et al.*, Rev. Mod. Phys. **57**, 61 (1985).

[11] C. V. Heer, Bull. Am. Phys. Soc. **6**, 58 (1961).

[12] J. E. Zimmermann and J. E. Mercereau, Phys. Rev. Lett. **14**, 887 (1965).

[13] L. A. Page, Phys. Rev. Lett. **35**, 543 (1975).

[14] J. Anandan, Phys. Rev. D **15**, 1448 (1977).

[15] S. A. Werner, J.-L. Staudenmann, and R. Colella, Phys. Rev. Lett. **42**, 1103 (1979).

[16] D. K. Atwood, M. A. Horne, C. G. Shull, and J. Arthur, Phys. Rev. Lett. **52**, 1673 (1984).

[17] F. Riehle, T. Kisters, A. Witte, J. Helmcke, and C. J. Bordé, Phys. Rev. Lett. **67**, 177 (1991); F. Riehle, A. Witte, T. Kisters, and J. Helmcke, Appl. Phys. B **54**, 333 (1992).

[18] A. W. Overhauser and R. Collela, Phys. Rev. Lett. **33**, 1237 (1974); R. Collela, A. W. Overhauser, and S. A. Werner, *ibid.* **34**, 1472 (1975).

[19] U. Bonse and T. Wroblewski, Phys. Rev. Lett. **51**, 1401

(1983).

[20] F. Hasselbach (unpublished).

[21] F. Hasselbach, German Patent No. DE 3504278 C2, February 2, 1985.

[22] F. Hasselbach and M. Nicklaus, J. Electron Microsc. (Tokyo) **35**, 691 (1986); in *Proceedings of the International Symposium on Electron Optics, Beijing, 1986*, edited by Ximen Jiye (Institute of Electronics, Academia Sinica, Beijing, 1987); Physica B **151**, 230 (1988).

[23] H. Ruder and H. Herold (private communication).

[24] These energy changes, which can occur in electrostatic electron optical components such as deflection elements or electron lenses, can reach values on the order of maximally 100 eV but are more typically on the order of a few eV (see Sec. III B and Ref. [75]). For this reason, we have not included electromagnetic potentials in the derivation of the Sagnac phase. For more complete Hamiltonians that include both acceleration and electromagnetic potentials, see, e.g., B. S. DeWitt, Phys. Rev. Lett. **16**, 1092 (1966); G. Papini, Nuovo Cimento B **52**, 136 (167); Ref. [60].

[25] E. J. Post, Rev. Mod. Phys. **39**, 475 (1967).

[26] J. Anandan, Phys. Rev. D **24**, 338 (1981).

[27] R. Rodloff, Z. Flugwiss. Weltraumforsch. **7**, 362 (1983).

[28] J. R. Wilkinson, Prog. Quantum Electron. **11**, 1 (1987).

[29] P. Langevin, C. R. Acad. Sci. **173**, 831 (1921); L. Silberstein, J. Opt. Soc. Am. **5**, 291 (1921); A. Ashtekar and A. Magnon, J. Math. Phys. **16**, 341 (1975).

[30] L. Stodolsky, Gen. Relativ. Gravitation **11**, 391 (1979).

[31] A. A. Logunov and Y. V. Chugreev, Usp. Fiz. Nauk **156**, 137 (1988) [Sov. Phys. Usp. **31**, 861 (1988)].

[32] A. C. Lunn, J. Opt. Soc. Am. **6**, 112 (1922).

[33] D. W. Allan, M. A. Weiss and N. Ashby, Science **228**, 69 (1985).

[34] D. Dieks and G. Nienhuis, Am. J. Phys. **58**, 650 (1990).

[35] F. W. Hehl and W.-T. Ni, Phys. Rev. D **42**, 2045 (1990).

[36] M. Dresden and C. N. Yang, Phys. Rev. D **20**, 1846 (1979).

[37] F. Aronowitz, in *Laser Applications*, edited by M. Ross (Academic, New York, 1971), Vol. I; H. J. Arditty and H. C. Lefevre, in *Fiber-Optic Rotation Sensors and Related Technologies*, Proceedings of the Ist International Conference MIT, Cambridge, Massachusetts, 1981 (Springer, New York, 1982), Vol. 32, p. 44; S. Ezekiel and H. J. Arditty, *ibid.*, Vol. 32, p. 2.

[38] H. C. Lefevre and H. J. Arditty, Appl. Opt. **21**, 1400 (1982).

[39] M. Nicklaus, Ph.D. thesis, University of Tübingen, Germany, 1989.

[40] J. L. Staudenmann, S. A. Werner, R. Collela and A. W. Overhauser, Phys. Rev. A **21**, 1419 (1980).

[41] C.-H. Tsai and D. Neilson, Phys. Rev. A **37**, 619 (1988).

[42] J. J. Sakurai, Phys. Rev. D **21**, 2993 (1980); B. H. W. Hendriks and G. Nienhuis, Quantum Opt. **2**, 13 (1990).

[43] B. Mashhoon, Phys. Rev. Lett. **61**, 2639 (1988).

[44] P. W. Forder, J. Phys. A **17**, 1343 (1984).

[45] F. Winterberg, Z. Naturforsch. **44a**, 1145 (1989).

[46] P. Hariharan, Appl. Opt. **14**, 2319 (1975).

[47] R. N. Henriksen and L. A. Nelson, Can. J. Phys. **63**, 1393 (1985).

[48] R. P. Feynman, R. B. Leighton, and M. Sands, *The Feynman Lectures of Physics* (Addison-Wesley, Reading, MA, 1969).

[49] P. Harzer, Astron. Nachr. **199**, 9 (1914); O. Knopf, Ann. Phys. (Leipzig) **62**, 389 (1920); W. R. Leeb, G. Schiffner, and E. Scheiterer, Appl. Opt. **18**, 1293 (1979).

[50] B. Prade and J.-Y. Vinet, Nuovo Cimento B **101**, 323 (1988).

[51] J. Anandan, Nuovo Cimento A **53**, 221 (1979); H.-H. Xu and C.-H. Tsai, Phys. Rev. A **41**, 4046 (1990).

[52] Y. Aharonov and D. Bohm, Phys. Rev. **115**, 485 (1959).

[53] W. Ehrenberg and R. E. Siday, Proc. Phys. Soc. London **62**, 8 (1949).

[54] R. Y. Chiao, in *Quantum Coherence*, Proceedings of the International Conference on Fundamental Aspects of Quantum Coherence, Columbia, SC, 1989, edited by J. S. Anandan (World Scientific, Singapore, 1990), p. 106.

[55] Recently, Aharonov and Anandan have generalized this concept by removing the adiabatic restriction and by replacing the parameter space by the notion of state space [Y. Aharonov and J. Anandan, Phys. Rev. Lett. **58**, 1593 (1987)].

[56] M. V. Berry, Proc. R. Soc. London Sect. A **392**, 45 (1984).

[57] H. J. Bernstein and A. V. Phillips, Sci. Am. **245**, 123 (1981).

[58] J. Anandan, in *Quantum Coherence* (Ref. [54]), p. ix.

[59] Y. Aharonov and G. Carmi, Found. Phys. **3**, 493 (1973); **4**, 75 (1974); J. H. Harris and M. D. Semon, *ibid.* **10**, 151 (1980).

[60] M. D. Semon, Found. Phys. **12**, 49 (1982).

[61] D. Dieks, Found. Phys. Lett. **3**, 347 (1990).

[62] R. Burghardt, Ann. Phys. (Leipzig) **40**, 140 (1983).

[63] A. Einstein, Ann. Phys. (Leipzig) **17**, 891 (1905).

[64] J. C. Hafele and R. E. Keating, Science **177**, 168 (1972).

[65] Y. Saburi, J. Radio Res. Lab. **23**, 255 (1976).

[66] A. V. Crewe, D. N. Eggenberger, J. Wall, and L. M. Welter, Rev. Sci. Instrum. **39**, 576 (1968).

[67] H. Hübner, Optik (Stuttgart) **63**, 179 (1983).

[68] I. L. Sokolovskaia, Zh. Tekh. Fiz. **26**, 1177 (1956) [Sov. Phys.—Tech. Phys. **1**, 1147 (1956)].

[69] F. Hasselbach and M. Nicklaus, J. Phys. E **17**, 782 (1984).

[70] G. Möllenstedt and H. Düker, Naturwissenschaften **42**, 41 (1955).

[71] G. Möllenstedt and H. Düker, Z. Phys. **145**, 377 (1956).

[72] J. Faget, Rev. Opt. Theor. Instrum. **40**, 347 (1961).

[73] H. Kaiser, S. A. Werner, and E. A. George, Phys. Rev. Lett. **50**, 560 (1983); A. G. Klein, G. I. Opat, and W. A. Hamilton, *ibid.* **50**, 563 (1983); W. A. Hamilton, A. G. Klein, and G. I. Opat, Phys. Rev. A **28**, 3149 (1983).

[74] G. Möllenstedt and G. Wohland, in *Proceedings of the VIIth European Congress on Electron Microscopy, Den Haag, 1980,* edited by P. Bredoro and G. Boom (Seventh European Congress on Electron Microscopy Foundation, Leiden, 1980).

[75] M. Nicklaus and F. Hasselbach, following paper, Phys. Rev. A **48**, 152 (1993).

[76] S. Nakadate, J. Opt. Soc. Am. A **5**, 1258 (1988).

[77] Reference [39]. The values reported there are slightly different from those reported here because a faulty field-emission extraction-voltage meter was detected only after the completion of the experiments. It had caused slightly wrong electron energies to be used in the calculation of the enclosed area A [see Eq. (24)].